

# Birefringent porous silicon membranes for optical sensing

Jesús Álvarez,<sup>1,\*</sup> Paolo Bettotti,<sup>2</sup> Isaac Suárez,<sup>1</sup> Neeraj Kumar,<sup>2</sup> Daniel Hill,<sup>1</sup> Vladimir Chirvony,<sup>1</sup> Lorenzo Pavesi,<sup>2</sup> and Juan Martínez-Pastor<sup>1</sup>

<sup>1</sup>UMDO, Materials Science Institute, University of Valencia, P.O. Box 22085, 46071 Valencia, Spain

<sup>2</sup>Nanoscience Laboratory, Department of Physics, University of Trento, via Sommarive 14, 38050 Povo-Trento, Italy

\*jesus.alvarez@uv.es

**Abstract:** In this work anisotropic porous silicon is investigated as a material for optical sensing. Birefringence and sensitivity of the anisotropic porous silicon membranes are thoroughly studied in the framework of Bruggeman model which is extended to incorporate the influence of environment effects, such as silicon oxidation. The membranes were also characterized optically demonstrating sensitivity as high as 1245 nm/RIU at 1500 nm. This experimental value only agrees with the theory when it takes into consideration the effect of silicon oxidation. Furthermore we demonstrate that oxidized porous silicon membranes have optical parameters with long term stability. Finally, we developed a new model to determine the contribution of the main depolarization sources to the overall depolarization process, and how it influences the measured spectra and the resolution of birefringence measurements.

©2011 Optical Society of America

**OCIS codes:** (260.1440) Birefringence; (290.5855) Scattering, polarization; (280.4788) Optical sensing and sensors.

---

## References and links

1. A. Jane, R. Dronov, A. Hodges, and N. H. Voelcker, "Porous silicon biosensors on the advance," *Trends Biotechnol.* **27**(4), 230–239 (2009).
2. X. D. Hoa, A. G. Kirk, and M. Tabrizian, "Towards integrated and sensitive surface plasmon resonance biosensors: a review of recent progress," *Biosens. Bioelectron.* **23**(2), 151–160 (2007).
3. S. Patskovsky, M. Meunier, P. N. Prasad, and A. V. Kabashin, "Self-noise-filtering phase-sensitive surface plasmon resonance biosensing," *Opt. Express* **18**(14), 14353–14358 (2010).
4. F. Prieto, L. Lechuga, A. Calle, A. Llobera, and C. Dominguez, "Optimized silicon antiresonant reflecting optical waveguides for sensing applications," *J. Lightwave Technol.* **19**(1), 75–83 (2001).
5. X. Wei and S. M. Weiss, "Guided mode biosensor based on grating coupled porous silicon waveguide," *Opt. Express* **19**(12), 11330–11339 (2011).
6. K. De Vos, I. Bartolozzi, E. Schacht, P. Bienstman, and R. Baets, "Silicon-on-Insulator microring resonator for sensitive and label-free biosensing," *Opt. Express* **15**(12), 7610–7615 (2007).
7. T. Claes, J. Molera, K. De Vos, E. Schacht, R. Baets, and P. Bienstman, "Label-Free Biosensing With a Slot-Waveguide-Based Ring Resonator in Silicon on Insulator," *IEEE Photon. J.* **1**(3), 197–204 (2009).
8. N. Skivesen, A. Têtù, M. Kristensen, J. Kjems, L. H. Frandsen, and P. I. Borel, "Photonic-crystal waveguide biosensor," *Opt. Express* **15**(6), 3169–3176 (2007).
9. T. Xu, N. Zhu, M. Y. Xu, L. Wosinski, J. S. Aitchison, and H. E. Ruda, "Pillar-array based optical sensor," *Opt. Express* **18**(6), 5420–5425 (2010).
10. C. Kang, C. T. Phare, Y. A. Vlasov, S. Assefa, and S. M. Weiss, "Photonic crystal slab sensor with enhanced surface area," *Opt. Express* **18**(26), 27930–27937 (2010).
11. O. Bisi, S. Ossicini, and L. Pavesi, "Porous silicon: a quantum sponge structure for silicon based optoelectronics," *Surf. Sci. Rep.* **38**(1–3), 1–126 (2000).
12. V. S. Lin, K. Motesharei, K. P. Dancil, M. J. Sailor, and M. R. A. Ghadiri, "A porous silicon-based optical interferometric biosensor," *Science* **278**(5339), 840–843 (1997).
13. V. Mulloni and L. Pavesi, "Porous silicon microcavities as optical chemical sensors," *Appl. Phys. Lett.* **76**(18), 2523–2525 (2000).
14. M. S. Salem, M. J. Sailor, K. Fukami, T. Sakka, and Y. H. Ogata, "Sensitivity of porous silicon rugate filters for chemical vapor detection," *J. Appl. Phys.* **103**(8), 083516 (2008).

15. T. Jalkanen, V. Torres-Costa, J. Salonen, M. Björkqvist, E. Mäkilä, J. M. Martínez-Duart, and V. P. Lehto, "Optical gas sensing properties of thermally hydrocarbonized porous silicon Bragg reflectors," *Opt. Express* **17**(7), 5446–5456 (2009).
16. E. Gross, D. Kovalev, N. Künzner, V. Y. Timoshenko, J. Diener, and F. Koch, "Highly sensitive recognition element based on birefringent porous silicon layers," *J. Appl. Phys.* **90**(7), 3529–3532 (2001).
17. M. Kompan, J. Salonen, and I. Shabanov, "Anomalous birefringence of light in free-standing samples of porous silicon," *J. Exp. Theor. Phys.* **90**(2), 324–329 (2000).
18. B.-H. O, R. Liu; Y. Y. Li, M. Sailor, and Y. Fainman, "Vapor sensor realized in an ultracompact polarization interferometer built of a freestanding porous-silicon form birefringent film," *IEEE Photo. Technol. Lett.* **15**(6), 834–836 (2003).
19. R. L. Smith and S. D. Collins, "Porous silicon formation mechanisms," *J. Appl. Phys.* **71**(8), R1–R22 (1992).
20. N. Künzner, D. Kovalev, J. Diener, E. Gross, V. Y. Timoshenko, G. Polisski, F. Koch, and M. Fujii, "Giant birefringence in anisotropically nanostructured silicon," *Opt. Lett.* **26**(16), 1265–1267 (2001).
21. N. Künzner, J. Diener, E. Gross, D. Kovalev, V. Y. Timoshenko, and M. Fujii, "Form birefringence of anisotropically nanostructured silicon," *Phys. Rev. B* **71**(19), 195304 (2005).
22. V. Y. Timoshenko, L. A. Osminkina, A. I. Efimova, L. A. Golovan, P. K. Kashkarov, D. Kovalev, N. Künzner, E. Gross, J. Diener, and F. Koch, "Anisotropy of optical absorption in birefringent porous silicon," *Phys. Rev. B* **67**(11), 113405 (2003).
23. J. E. Sipe and R. W. Boyd, "Nonlinear susceptibility of composite optical materials in the Maxwell Garnett model," *Phys. Rev. A* **46**(3), 1614–1629 (1992).
24. H. Looyenga, "Dielectric constants of heterogeneous mixtures," *Physica* **31**(3), 401–406 (1965).
25. T. C. Choy, "Effective Medium Theory, Principles and Applications," Oxford University Press, (1999).
26. K. Nishida, M. Fujii, S. Hayashi, and J. Diener, "Temperature dependence of optical anisotropy of birefringent porous silicon," *Appl. Phys. Lett.* **96**(24), 243102 (2010).
27. V. Kochergin, M. Christophersen, H. Föll, "Effective medium approach for calculations of optical anisotropy in porous materials," *Appl. Phys. B* **79**, 731–739 (2004).
28. K. A. Kilian, T. Böcking, and J. J. Gooding, "The importance of surface chemistry in mesoporous materials: lessons from porous silicon biosensors," *Chem. Commun. (Camb.)* (6): 630–640 (2009).
29. I. Suárez, V. Chirvony, D. Hill, and J. Martínez-Pastor, "Simulation of surface-modified porous silicon photonic crystals for biosensing applications," *Phot. Nano. Fund. Appl.*, doi:10.1016, (2011)
30. M. Ghulinyan, C. J. Oton, G. Bonetti, Z. Gaburro, and L. Pavesi, "Free-standing porous silicon single and multiple optical cavities," *J. Appl. Phys.* **93**(12), 9724–9729 (2003).
31. A. E. Pap, K. Kordás, T. F. George, and S. Leppävuori, "Thermal Oxidation of Porous Silicon: Study on Reaction Kinetics," *J. Phys. Chem. B* **108**(34), 12744–12747 (2004).
32. S. M. Nee, "Depolarization and retardation of a birefringent slab," *J. Opt. Soc. Am. A* **17**(11), 2067–2073 (2000).
33. K. H. Jun and K. S. Lim, "Simulation of the depolarization effect in porous silicon," *Appl. Opt.* **42**(7), 1211–1215 (2003).

---

## 1. Introduction

During the last decade the development of optical sensors has been pursued by many research groups due to the need for simple, low cost, fast and accurate substance identification in applications such as clinical diagnosis, food safety, environmental monitoring and homeland security [1]. To this end, various materials and detection mechanisms such as Surface Plasmon Resonance (SPR) [2,3], photonic waveguides [4,5], microring resonators [6,7], and photonic crystals [8–10] have been designed and implemented as optical sensors.

Porous Silicon (PSi) has unique properties for sensing application due to its morphological structure that presents a large surface area/volume ratio, adjustable porosity, pore sizes and layer thickness [11]. Moreover its low cost fabrication process and its compatibility with microfabrication technologies make possible to use it for the fabrication of highly integrated sensors. In consequence, several interferometric schemes using (100) PSi have been proposed for optical sensors [12–15]. PSi made from (110) Si wafers however, presents very high birefringence values, which is very sensitive to the presence of different substances within its pores [16–18]. The use of this anisotropic PSi together with optical polarimetric schemes for measurement of birefringence therefore makes it an ideal candidate for commercially viable highly sensitive optical sensors.

In this work PSi membranes produced from (110) surface oriented silicon are evaluated as a material for sensing applications. Firstly, in section 2 a theoretical study of the birefringence and sensitivity of the membranes is presented. For this purpose, we extend the binary

Bruggeman model used in literature by including an important external effect in PSi such as the oxidation of the pore surface walls. Then, the changes in the birefringence from filling the pores by different substances are calculated theoretically. Section 3 describes the fabrication process for anisotropic PSi membranes with different pore sizes and thicknesses, with and without a post thermal oxidation process. Section 4 reports the optical characterization of the samples when the pores are filled by different liquids. Birefringence measurements are only found to be in good agreement with those predicted by the model when the effect of silicon oxidation is considered. It is remarkable to say that these measurements show long time stability, with the thermal oxidation having reduced drift. Within these birefringence sensitivities of the membranes are found to be as high as 1250nm/RIU at 1500 nm. Finally, in Section 5 depolarization is identified as the cause of the discrepancies between measured and theoretical spectra. These discrepancies have already been found in previous work; however, to the best of our knowledge, it is the first time when they are studied. The three main factors contributing to the depolarization were found to be: spectrometer bandwidth, thickness variations of PSi and scattering. Using a novel developed statistical model the contribution of each factor to the total depolarization is identified by fitting the measured spectra to the theoretical one. This model also allows obtaining the standard deviation of the measured birefringence.

## 2. Theoretical

Bulk silicon is an isotropic material due to its diamond cubic crystal structure, however PSi prepared from (110) Si surface oriented substrates presents a high anisotropy due to pores grow preferentially along the [100] and [010] crystallographic directions [19], as seen in Fig. 1. The orientation of the pores along those directions results in a difference in the refractive indices along the [001] and the  $[\bar{1}\bar{1}0]$  directions [20].

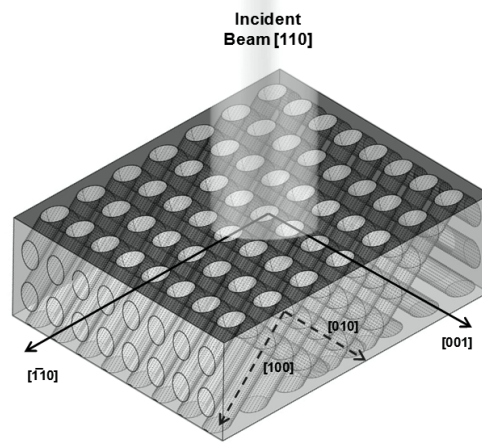


Fig. 1. Scheme of an anisotropic PSi layer produced from a (110) surface oriented Si wafer.

In accounting for the anisotropic microstructure of this type of PSi, the pores are modeled as ellipsoids of revolution with their axes of symmetry aligned along the [001] direction and the  $[\bar{1}\bar{1}0]$  direction lying on the (110) surface plane. The depolarization factors,  $L_{[001]}$  and  $L_{[\bar{1}\bar{1}0]}$ , describe the screening efficiency of external electromagnetic fields inside the ellipsoids, characterizing the optical properties of the PSi layer. Their values are given by Eq. (1) and Eq. (2) [21,22]:

$$L_{[\bar{1}\bar{1}0]} = \frac{1}{1-\xi^2} \left( 1 - \xi \cdot \frac{\arcsin(\sqrt{1-\xi^2})}{\sqrt{1-\xi^2}} \right) \quad (1)$$

$$L_{[001]} = \frac{1 - L_{[\bar{1}\bar{1}0]}}{2} \quad (2)$$

where  $\xi = a/b$ , being  $a$  and  $b$  the major and minor ellipse axes respectively. As the directions [100] and [010] form an angle of  $50.77^\circ$  with respect to the normal plane (110) [19], the ratio  $\xi$  has a value of 0.7746. Substituting this value into Eq. (1) and (2) depolarization factors of  $L_{[001]}$  equal to 0.2938 and  $L_{[\bar{1}\bar{1}0]}$  equal to 0.4035 are obtained.

Among the various methods that can be used to estimate the birefringence of an anisotropic PSi layer, such as the Maxwell-Garnett theory [23], the Looyenga method [24] or the Bruggeman model [25], for this work the Bruggeman model was chosen since for samples with porosities below 0.8 it provides more accurate predictions than the other methods [26,27]. The only assumption made by this model is the static electric field condition, which is satisfied when wavelength of light is much longer than the transverse pore size. As is described in section 3, fabricated samples have porosities below 0.8 and pore diameters smaller than 100 nm, fulfilling the static electric field condition. The Bruggeman model is described by Eq. (3):

$$\sum_i f_i \frac{n_i^2(\lambda) - n_{[001],[110]}^2}{n_{[001],[110]}^2 + L_{[001],[110]} \cdot (n_i^2(\lambda) - n_{[001],[110]}^2)} = 0 \quad (3)$$

where  $f_i$  is the volume fraction of the different materials that form the PSi membrane,  $n_i(\lambda)$  their refractive indices, and  $L_{[001]}$  and  $L_{[\bar{1}\bar{1}0]}$  the previously described depolarization factors. The unknown  $n_{[001]}$  and  $n_{[\bar{1}\bar{1}0]}$  are the refractive indices along the main axes and are related to the birefringence by means of  $\Delta n = n_{[001]} - n_{[\bar{1}\bar{1}0]}$ . Equation (3) can be solved using numerical methods.

### 2.1 PSi birefringence and sensitivity

The main objective in using PSi for polarimetry based sensing is to maximize the birefringence change coming from the presence of different substances filling the pores. For this purpose Eq. (3) was solved for wavelengths from 600 nm to 1600 nm and porosities ranged from 0 to 1. It was considered a binary PSi layer composed by silicon and empty pores ( $n_{\text{Pore}} \approx 1$ ). The results of the calculated birefringence are displayed in Fig. 2 (a).

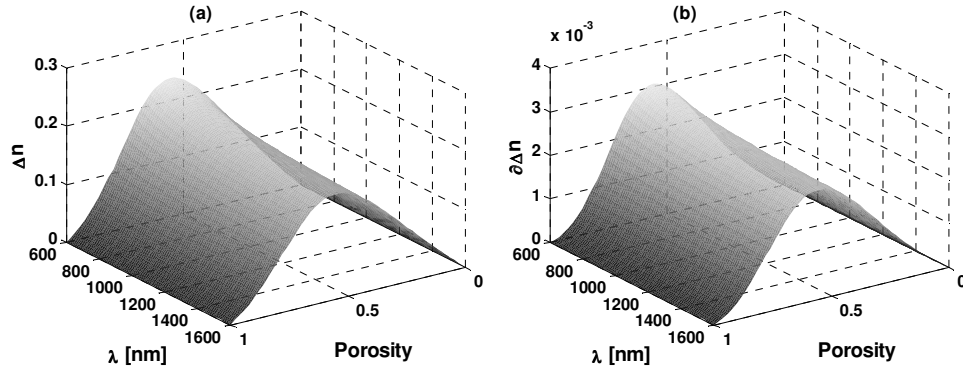


Fig. 2. (a) Birefringence computed using the Bruggeman model for a binary PSi layer (silicon and pores filled with air) as a function of wavelength and porosity. (b) Birefringence change due to presence of different substances inside the pores (ethanol and isopropanol) as a function of wavelength and porosity.

Two clear observations can be made. First, it can be noted that birefringence has a maximum for a porosity of 0.55. Secondly, it decreases with wavelength, following the behavior of silicon refractive index.

In a second step the birefringence change when pores are filled by different material is simulated. For this purpose, Eq. (3) was solved for the pores being filled with ethanol ( $n_{Pore} \approx 1.36$ ) and isopropanol ( $n_{Pore} \approx 1.377$ ). Birefringence changes due to refractive index changes within the pores ( $\partial\Delta n = \Delta n|_{n_{Pore}=1.36} - \Delta n|_{n_{Pore}=1.377}$ ) are shown in Fig. 2 (b). Like in the case of filling the pores by air, the maximum birefringence change is seen for a porosity of 0.55. It can therefore be concluded that in order to have an efficient PSi membrane sensor, the refractive index contrast must be as high as possible and porosity should be as near to 0.55 as fabrication permits.

## 2.2 Effect of silicon oxidation

The internal pore surfaces of freshly prepared PSi are prone to oxidize under ambient conditions leaving a thin  $\text{SiO}_2$  layer over recently etched PSi pores, see Fig. 3 (a). Furthermore, in order to stabilize the surface and avoid changes in the PSi during sensing the silicon dioxide layer is purposely increased via a thermal oxidation process [28]. Here, the effect that this silicon dioxide layer has over the birefringence is modeled by including its volume fraction in Eq. (3). Thus, a three component medium has now been formed consisting of silicon, silicon dioxide and pores. The bonding of silicon with oxygen produces a 2.27 fold increase in volume over bulk silicon, so silicon oxidation produces a reduction of pores and silicon volume fractions [29]. The new volume fractions of silicon and pores are related to the silicon dioxide volume fraction by Eq. 4 and 5 respectively:

$$f_{Si} = f_{Si_0} - f_{SiO_2} / 2.27 \quad (4)$$

$$f_{Pores} = f_{Pores_0} - 1.27 / 2.27 \cdot f_{SiO_2} \quad (5)$$

where  $f_{Si_0}$  and  $f_{Pores_0}$  denotes the volume fraction of the silicon and pores prior to oxidation. The effect that grown silicon dioxide has over the birefringence is depicted in Fig. 3 (b). As can be seen, silicon dioxide reduces the birefringence for porosities above 0.33. This reduction in birefringence is attributed to the decrease of the index contrast between the initial PSi layer, and the same layer after the oxidation process. For porosities below 0.33 the

volume fraction of silicon is so high that its oxidation causes an increase in the index contrast, and then, a small increment in the birefringence value.

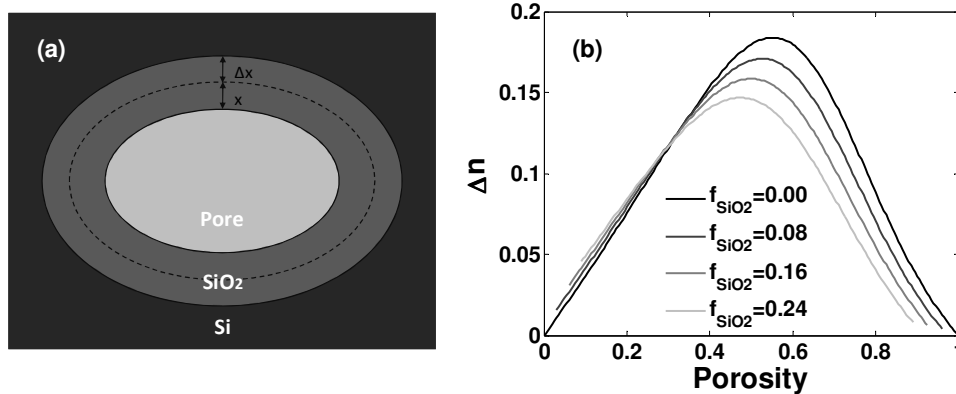


Fig. 3. (a) Pore cross-section scheme. The surface oxidation of the pores walls leads to a volume expansion (dashed line). (b) Birefringence variation as a function of the PSi layer porosity for several silicon dioxide volume fractions.

### 3. Fabrication

The PSi birefringent properties were characterized for a set of samples consisting of nanoporous silicon etched into p-type (110) Si with resistivity of 0.01-0.001 Ohm/cm. Pores sizes were in the range of few tens of nanometers, as shown in Fig. 4. Samples were prepared by electrochemical etching using a solution composed of HF:Ethanol = 3:7 by volume, considering an initial HF concentration of 48%. A current density of 25 mA/cm<sup>2</sup> was used during the etching.

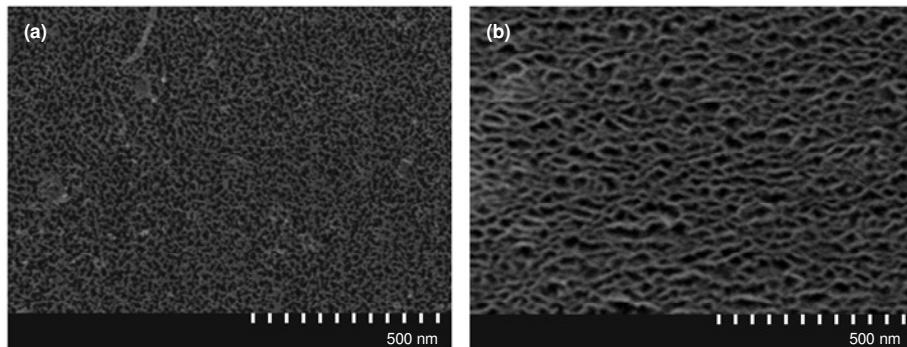


Fig. 4. Surface SEM images of two fabricated and optically characterized samples: (a) PSi sample with pore size in the order of a 10 nm, (b) PSi sample with pores size in the order of 50 nm.

For subsequent optical characterization, porous membranes were detached from the bulk silicon layer that supports them by applying a strong current burst at the end of the etching completely dissolving the bottom silicon layer that surrounds the etched area. With this procedure the membrane can be transferred to another substrate. More details can be found in [30]. Several (110) PSi membranes of various thicknesses were fabricated and transferred to a glass substrate in which a 3-4 mm circular hole was made in order to characterize the birefringence and depolarization effects as a function of optical path.

Before measuring the birefringence of the fabricated samples, a thermal oxidation at 200°C for 12 hours was carried out in order to stabilize pore surfaces during the

measurements. At this temperature, after 12 hours, the silicon dioxide grown has already saturated to a volume fraction ratio of 0.16 ( $f_{SiO_2} / f_{Si} = 0.16$ ) [31].

#### 4. Experimental and results

The optical anisotropy of fabricated samples was determined by analyzing the state of polarization of the light transmitted through them. The setup depicted in Fig. 5 shows how the output light from a tungsten halogen lamp is collimated and then polarized linearly at  $45^\circ$  with respect to the horizontal direction. The linearly polarized light passes through the anisotropic PSi sample which is oriented with its [001] and  $[\bar{1}\bar{1}0]$  crystallographic directions parallel to the vertical and horizontal directions, respectively. The lamp spot in the position where the PSi samples are placed had a size of 1.2 mm with a divergence of  $1^\circ$ . The components of light along the [001] and  $[\bar{1}\bar{1}0]$  directions experiment a phase shift given by:

$$\Delta\phi(\lambda) = \frac{2\pi}{\lambda} \cdot d \cdot \Delta n(\lambda) \quad (6)$$

where  $\lambda$  is the incident wavelength of light,  $d$  the PSi membrane thickness and  $\Delta n(\lambda)$  its birefringence. The phase shift is converted into an amplitude shift through traversing a second polarizer (usually called analyzer), which is then recorded by a spectrometer. To cover the transmission spectrum in the whole region of interest, from 600 to 1600 nm, the spectrometers used were an Ocean Optics NIR512 with a bandwidth of 3.1 nm and an Ocean Optics RedTide 650 with a bandwidth of 2 nm.

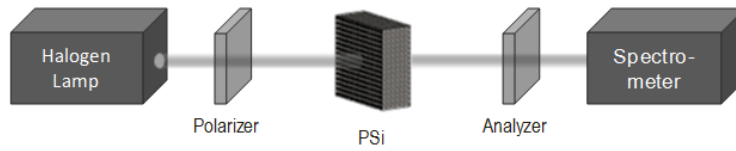


Fig. 5. Scheme of the setup used for the optical characterization of the PSi membranes.

The normalized transmittance (light recorded in the parallel or cross direction divided by the sum of the light in the parallel and cross directions) for polarizers placed in parallel or crossed is given by:

$$T_{\parallel}(\lambda) = \cos^2(\Delta\phi(\lambda)/2) \quad (7)$$

$$T_{\perp}(\lambda) = \sin^2(\Delta\phi(\lambda)/2) \quad (8)$$

where  $\Delta\phi(\lambda)$  is the phase retardation given by Eq. (6).

##### 4.1. Sensitivity

The sensitivity of the PSi membranes was determined by filling the samples with the different liquids studied in section 2 and then measuring the shift produced in the transmission spectrum. For this purpose we placed a thermally treated PSi sample in a flow cell made from optical glass. This flow cell was then filled with ethanol ( $n_{Etha} \approx 1.36$ ) and isopropanol ( $n_{Isop} \approx 1.377$ ). A few seconds after filling the flow cell with the liquids, the transmission spectra stabilize, indicating that the liquids had completely filled the pores. Figure 6 (a) shows the values of  $T_{\perp}(\lambda)/T_{\parallel}(\lambda)$  versus wavelength for a thermally oxidized PSi sample with a thickness of 30  $\mu\text{m}$  when the pores are empty (red line), when filled with isopropanol (green

line) or ethanol (blue line). From this graph, the birefringence was obtained and is depicted in Fig. 6 (b). A blue shift in the  $T_{\perp}(\lambda)/T_{\parallel}(\lambda)$  can be clearly seen in Fig. 6 (a) that is associated with the birefringence change seen in Fig. 6 (b). The birefringence change between the samples filled with isopropanol and filled with ethanol was obtained from the curves fitted to experimental birefringence values depicted in Fig. 6 (b). These values are  $1.8 \times 10^{-3}$ ,  $1.1 \times 10^{-3}$ , and  $0.98 \times 10^{-3}$  for the wavelengths of 810, 1300 and 1500 nm respectively. The values predicted in the model proposed in section 2 when a silicon oxide volume fraction of 0.16 was considered were  $1.3 \times 10^{-3}$  at 810 nm, and  $1.2 \times 10^{-3}$  at 1300 and 1500 nm. Then, the model for estimating the optical sensitivity of a PSi membrane in a polarimetric scheme is thereby validated with the effect of silicon oxidation found to be a critical parameter.

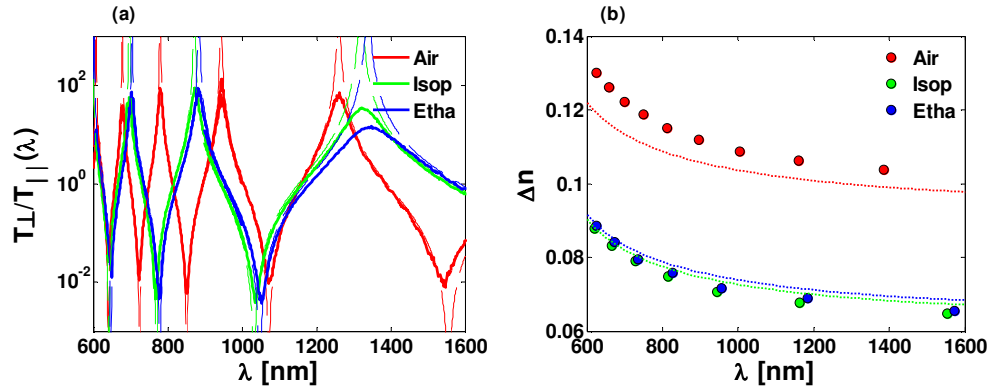


Fig. 6. (a) Transmission spectra for empty pores (red line), pores completely filled with isopropanol (green line) and ethanol (blue line). Dashed lines represent the corresponding theoretical curves. (b) Birefringence data obtained from the measured spectra (dots) and simulated curves using the Bruggeman model (dashed lines) for air (red), isopropanol (green) and ethanol (blue).

In order to compare PSi membranes with other sensing platforms, optical sensitivity was obtained in terms of nm per Refractive Index Unit (RIU). This calculation was done by dividing the measured blueshift by the refractive index change ( $n_{IPA} - n_{ETHA} = 0.017$ ) from the spectra and data shown in Fig. 6 (a)-(b). In this way, the anisotropic PSi membranes exhibit sensitivities of 626 nm/RIU at 810 nm, 1135 nm/RIU at 1300 nm and 1247 nm/RIU at 1500 nm. In comparison, for microring resonators made in SOI, sensitivities of 293 nm/RIU for bulk refractive index measurements were reported [7], whilst for photonic crystals made from Si pillars in a SiO<sub>2</sub> substrate, sensitivities of 350 nm/RIU were reported [9]. Therefore, the sensitivity provided by our anisotropic PSi membranes indicates their high potential for chemical and biomolecular sensing applications.

#### 4.2. PSi stability over time

An important issue for optical sensors is the stability of their properties with time. In order to characterize this limitation in our PSi membranes an experiment was carried out to determine the drift of the birefringence over time. Two PSi samples were used for this purpose, both of them with similar pore diameters. The first sample consisted of a porous silicon membrane without any thermal treatment. The second one was thermally oxidized in an oven at 200 °C during twelve hours. The birefringence of both samples was measured immediately after the fabrication process, and again one hundred and fifteen days later (Fig. 7). The variation of the birefringence for the first sample is equal to  $1.2 \times 10^{-2}$  RIU at 1500 nm, corresponding to a birefringence drift of  $7 \times 10^{-8}$  RIU/min. For the thermally treated sample, the birefringence

variation is approximately seven times less at  $1.6 \times 10^{-3}$  RIU at 1500 nm, corresponding to a drift of  $9 \times 10^{-9}$  RIU/min.

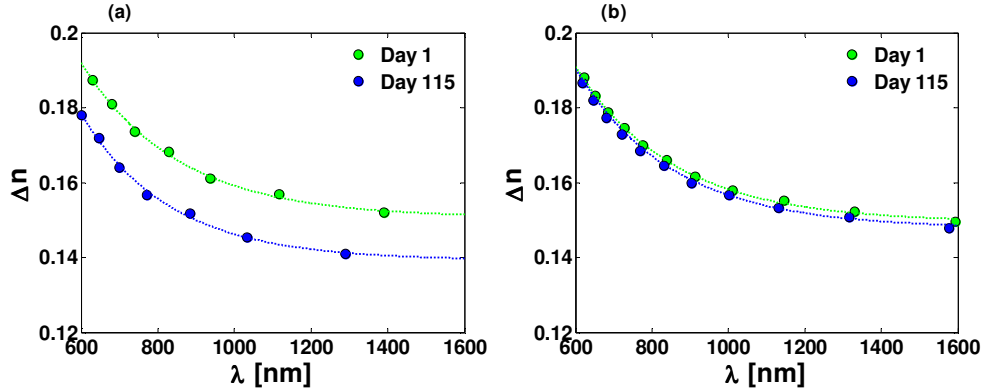


Fig. 7. Birefringence measured immediately after samples fabrication (green dots) and one hundred fifteen days later (blue dots) for a PSi sample without thermal treatment (a) and for a sample oxidized at 200° during 12 hours (b).

## 5. Depolarization effects in anisotropic PSi

Although poles and zeros (ideal theoretical curves shown in Fig. 6 (a) by dashed lines) are expected when  $T_{\parallel}(\lambda)$  and  $T_{\perp}(\lambda)$  are respectively zero in Eqs. (7-8), we observed in Fig. 6 (a) that local maxima and minima values of  $10^2$  and  $10^{-2}$  were measured, respectively. Depolarization is known to be the cause of the difference between the ideal response and that measured [32]. The depolarization represents the degree of random polarization during the measurement process. In the birefringence measurements of PSi membranes, we identify the three main sources of depolarization to be: (1) spectrometer bandwidth, (2) thickness variations in the PSi membrane across the light spot area and (3) light scattering produced by pores with a random spatial distribution:

(1) The spectrometer bandwidth affects the phase retardation in two different ways. First the quasi-monochromatic waves superimpose incoherently providing different phase retardation values for each wave. Secondly, since the PSi birefringence is wavelength dependent, light waves with different wavelengths have different birefringence.

(2) Phase retardation is a function of sample thickness and so thickness variations across the spot area will result in superimposing waves that see different thicknesses of the sample.

(3) Volume scattering in the inhomogeneous medium of PSi generates incoherent light which also contributes to the depolarization process [33].

We take into account the previously described effect by modeling the phase retardation as a stochastic process where each of the light waves that pass through the porous silicon has a phase retardation given by:

$$\Delta\phi_s(\lambda) = \frac{2\pi}{\lambda + \Lambda} \cdot (d + \Gamma) \cdot \Delta n(\lambda + \Lambda) + \Psi \quad (9)$$

where  $\Lambda$ ,  $\Gamma$  and  $\Psi$  are random variables with a Gaussian distribution whose most probable values are zero; and their standard deviation correspond to the above described effects (1)-(3):  $\Lambda$  represents the variance in the wavelength due to the effect of the spectrometer bandwidth,  $\Gamma$  represents the irregularities in the porous silicon samples thickness and  $\Psi$  represents the contribution of the scattering to the depolarization process.

From Eq. (9) the normalized transmittance for the parallel and crossed polarizers is obtained by means of averaging an infinite (or high enough) number of light waves whose phase retardation is the random variable declared in Eq. (9). Those averaged transmittances can be thus calculated by the expressions:

$$T_{\parallel}(\lambda) = \lim_{N \rightarrow \infty} \left( \frac{1}{N} \sum_1^N \cos^2(\Delta\phi_s(\lambda)/2) \right) \quad (10)$$

$$T_{\perp}(\lambda) = \lim_{N \rightarrow \infty} \left( \frac{1}{N} \sum_1^N \sin^2(\Delta\phi_s(\lambda)/2) \right) \quad (11)$$

Using Eq. (10) and Eq. (11), the depolarization effect observed in the PSi membrane measurements were evaluated. Since the bandwidth of the spectrometer is known, and equal to 2 nm for 600-1000 nm and 3.1 nm for 1000-1600 nm, the standard deviation of the variables  $\Gamma$  and  $\Psi$  could be obtained by fitting calculated spectra from Eq. (10) and 11 to the measured spectrum. Figure 8 (a) displays the  $T_{\perp}(\lambda)/T_{\parallel}(\lambda)$  measured spectra and the simulated one from the previously described model for a 30  $\mu\text{m}$  thickness sample. The best fitting between the experimental data and the simulation was obtained for standard deviations of  $\Gamma$  and  $\Psi$  equal to 100 nm and 0.13 rad, respectively. Figure 8 (b) displays the measured and simulated spectra of a 64  $\mu\text{m}$  thick PSi sample. In this case, the experimental data was fitted with standard deviations of  $\Gamma$  and  $\Psi$  of 100 nm and 0.3 rad, respectively. In other samples, the standard deviation of  $\Gamma$  was always found to be equal to 100 nm. However in the case of  $\Psi$  its standard deviation clearly increases with sample thickness.

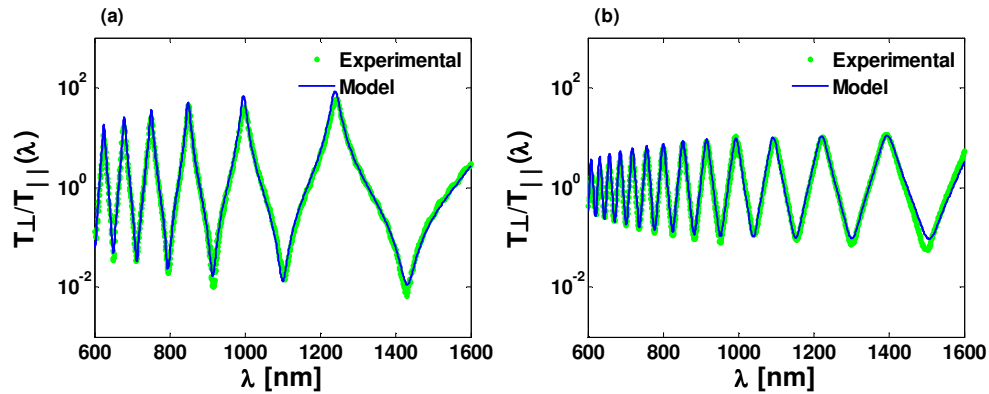


Fig. 8. (a) Measured (green line) and fitted transmittance spectra (dotted blue line) for a PSi sample with thickness of 30  $\mu\text{m}$  (a) and a PSi sample with thickness of 64  $\mu\text{m}$  (b).

A consequence of the depolarization process is the spreading of the phase retardation given by Eq. (9). These uncertainties in the phase retardation produced by the depolarization will be related with the resolution in the measurement of the PSi samples birefringence. Theoretically, in an ideal system where there is no depolarization, the resolution of phase retardation (or birefringence) measurements is determined solely by the instrumentation limits. In reality since depolarization characterizes the randomness of the measurement process the resolution of phase retardation measurements will be related to depolarization.

Figure 9 (a) and (b) show the probability density function of the birefringence calculated from Eq. (6) when the effect that depolarization has over the phase retardation is taken into account for the 30  $\mu\text{m}$  and 64  $\mu\text{m}$  samples, respectively. Comparing both graphs we can see that the main contribution to the total depolarization is the depolarization caused by the scattering. It can be concluded that for both samples the main source of the depolarization is the light scattering by the pores being more important for thicker samples, as expected. The

depolarization process affects the measurement birefringence by increasing its standard deviation, which reduces the precision of the measured value.

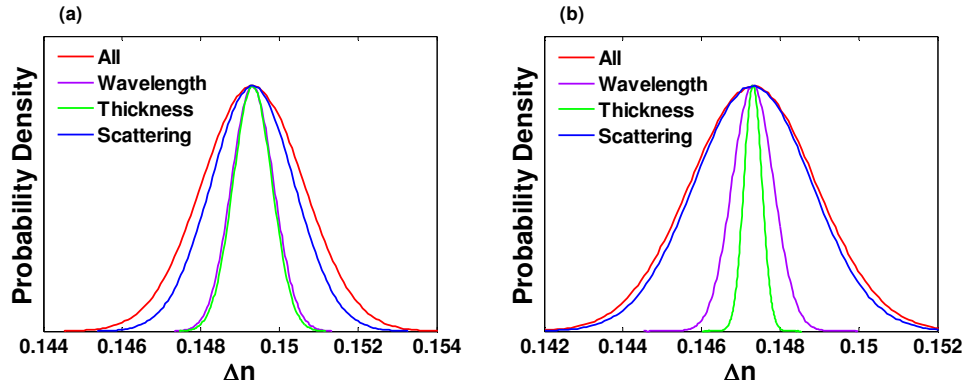


Fig. 9. (a) Birefringence probability density functions in account for the three main factors that produces the depolarization for a 30  $\mu\text{m}$  thick sample (a) and a 64  $\mu\text{m}$  thick sample (b).

## 6. Conclusion

The modeling, fabrication and characterization of PSi membranes made from (110) silicon was reported. Based on the Bruggeman model the theoretical birefringence and sensitivity was obtained as a function of the porosity and wavelength, with both values have a maximum shown for porosities of 0.55. The impact that the oxidation of pore walls has on birefringence and sensitivity was also studied theoretically. Thereafter a set of PSi samples with different pore sizes and thicknesses were fabricated and characterized. Experimentally determined values of birefringence were obtained for samples filled with air, ethanol and isopropanol, obtaining a sensitivity of 1247 nm/RIU at 1500 nm. This experimental value were found to be in good agreement with the value obtained theoretically by using the model described in section 2 when the effect of silicon oxidation is taken into account. The final part of the work identifies the effect of depolarization for difference between the theoretical spectra and those measured. A statistical model was demonstrated that takes into account the main depolarization sources such as the spectrometer bandwidth, the surface thickness variation and the scattering. With this model it was possible to obtain the standard deviations of the variables that are used to model each of the depolarization sources, as well as the standar deviation of the birefringence measured value.

## Acknowledgments

This work was supported by EC through the project FP7-257401 POSITIVE.